Applied Physics Letters

RESEARCH ARTICLE | JUNE 05 2023

A high-performance thermal transistor based on interfacial negative differential thermal resistance

Yu Yang ; Yunshan Zhao ; Lifa Zhang

Appl. Phys. Lett. 122, 232201 (2023)
https://doi.org/10.1063/5.0149544

Applied Physics Letters ARTICLE pubs.aip.org/aip/apl

A high-performance thermal transistor based on interfacial negative differential thermal resistance

Cite as: Appl. Phys. Lett. **122**, 232201 (2023); doi: 10.1063/5.0149544
Submitted: 7 March 2023 · Accepted: 15 May 2023 ·
Published Online: 5 June 2023

Yu Yang, Yunshan Zhao,[a] and Lifa Zhang[a]

AFFILIATIONS

Phonon Engineering Research Center of Jiangsu Province, Center for Quantum Transport and Thermal Energy Science, Institute of Physics Frontiers and Interdisciplinary Sciences, School of Physics and Technology, Nanjing Normal University, Nanjing 210023, China

[a]Authors to whom correspondence should be addressed: phyzys@njnu.edu.cn and phyzlf@njnu.edu.cn

ABSTRACT

A thermal transistor, which can achieve the smart, flexible, and precisely controlled thermal management, proves to be a promising thermal device. Recently, thermal transistors based on the negative differential thermal resistance (NDTR) have been regarded as the most feasible configuration considering their simple structures. Among the several methods to implement NDTR, the method of reducing the contact pressure between mated surfaces by using the negative thermal expansion material, thus generating a negative temperature dependent interface thermal conductance and accompanied NDTR, is the most likely to be observed experimentally. In this paper, a thermal transistor based on NDTR is designed by engineering the interfacial thermal resistance. Moreover, we optimize the switching function and the amplification function of the transistor by only adjusting the temperature and the length of the source terminal. As an example, a silicon thermal transistor with a high switching ratio as well as an accurately controlled thermal flux amplification function is discussed at low temperature. The design and optimization of macroscopic thermal transistor will promote the rapid development of thermal functional devices and help to control thermal flux in a more flexible and effective way.

The waste heat generated from micro- to macro-scale attracts more and more attention, and the effective control of thermal flux is, thus, particularly important, especially for the chip industry,[1] the new energy vehicle industry,[2] etc. In order to solve the issue of waste heat, researchers have proposed various strategies to achieve high-performance thermal controls,[3–5] such as thermal metamaterials,[6–8] phononic crystals,[9,10] thermal diodes,[11–16] thermal transistors,[17–35] etc. Among the various thermal management methods, thermal transistors have become a research hotspot in recent years because of their advantages of being most flexible, wide application, and most complete functions. In 2006, the first thermal transistor was theoretically proposed by Li *et al.* in the Frenkel-Kontorova (FK) model,[17] and then different kinds of thermal transistors were proposed subsequently, such as thermal transistor based on atomic chain model,[17–19] near-field radiation thermal transistor,[20–22] quantum thermal transistors,[23–34] and Josephson junction thermal transistor.[35]

Similar to the electronic transistor, the thermal transistor proposed is mainly based on the negative differential thermal resistance (NDTR),[17–19,23–50] which refers to the phenomenon that the thermal flux decreases when the temperature bias increases in some particular systems. Recently, a three-terminal magnetic thermal transistor has been experimentally implemented in which the NDTR is achieved by a gate-temperature dependent magnetic thermally conducting shuttle.[51] A similar design achieves NDTR in a one-dimensional thermal transport system by controlling the on-off of thermal flux with the temperature-dependent shape memory alloys.[52] However, these kinds of NDTR mainly come from a drastic temperature-dependent phase transition, which can achieve an excellent thermal switching function, but it is difficult to achieve an accurately controlled thermal amplification function because the temperature region of phase transition is too small. In addition to taking advantage of phase transition properties, the other studies about the NDTR were mainly based on the atomic chains model,[17–19,36–47] nanostructures,[35,48–50] or small quantum systems.[23–34] Although they have large temperature region of NDTR, they are either too simplistic or requiring extreme experimental conditions, such as extremely low temperature and extremely small size.

Following the research of He *et al.* on the atomic chain model,[40] Yang *et al.* designed a new scheme to realize NDTR in the negative thermal expansion (NTE) materials based on the temperature-dependent interfacial thermal resistance (ITR),[53–55] which arises from the temperature-dependent NTE breaking the interfacial pressure and is particularly promising to observe the NDTR in macroscopic experiments.[56,57]

In this work, the macroscopic thermal transistor based on the interfacial NDTR (INDTR) has been designed and optimized. It was found that the INDTR could occur and can be used to fabricate thermal transistor when the interfacial thermal conductance (ITC) has a more than linear negative and concave function of temperature near the temperature of the drain terminal T_D. Then, by adjusting the temperature of the source terminal T_S and the length of the source material L_S, a thermal transistor with the optimal switching function and amplification function can be realized. Finally, a silicon homojunction thermal transistor with both the good switching function and amplification function is discussed at low temperature.

First of all, the form of ITC that can be used to realize the INDTR is discussed. According to Fourier's law, the thermal flux J through the material can be described as

$$J = -\frac{1}{L}\int_{T_D}^{T_S} \kappa(T)\ dT. \tag{1}$$

In general, the thermal conductivity of the one material should be a positive value; hence, the thermal flux through the material increases as the external temperature difference increases. Here, L and $\kappa(T)$ are the length and temperature dependent thermal conductivity of the material, respectively, and T_S and T_D are the temperature of the source terminal and the drain terminal at both ends of the material, respectively. Therefore, the opposite NDTR is usually realized in the multi-junction system with interfaces, since it is difficult to obtain a temperature-sensitive and drastically changing thermal resistance in a single material. The thermal flux in a multi-junction system with ITC can also be expressed according to Fourier's law as

$$J = \frac{1}{L_D}\int_{T_D}^{T_{mD}} \kappa_D(T)\ dT = \frac{(T_{mS} - T_{mD})}{R_i(T_{mS}, T_{mD})} = \frac{1}{L_S}\int_{T_{mS}}^{T_S} \kappa_S(T)\ dT, \tag{2}$$

where D and S represent the drain terminal and the source terminal, respectively. The $\kappa_D(T)$, $\kappa_S(T)$, L_D, and L_S denote the temperature-dependent thermal conductivity and length for material of drain and material of source, respectively. The T_{mD} and T_{mS} represent the temperature at the surfaces of the interface near the drain and source, respectively. The $R_i(T_{mS}, T_{mD})$ represents the total thermal resistance of the interface. In 2020, Yang *et al.* proposed a highly sensitive temperature-dependent ITC (TDITC) in the NTE materials, which is promising to achieve the INDTR[56] in the actual macrosystem (see Sec. S1 in the supplementary material for detailed discussions about the INDTR and TDITC). To find out the necessary conditions for INDTR occurred in actual homogeneous and heterogeneous systems, we constructed a homojunction model with various ITCs, as shown in Fig. 1(a). The function expressions for various ITCs are listed on the right

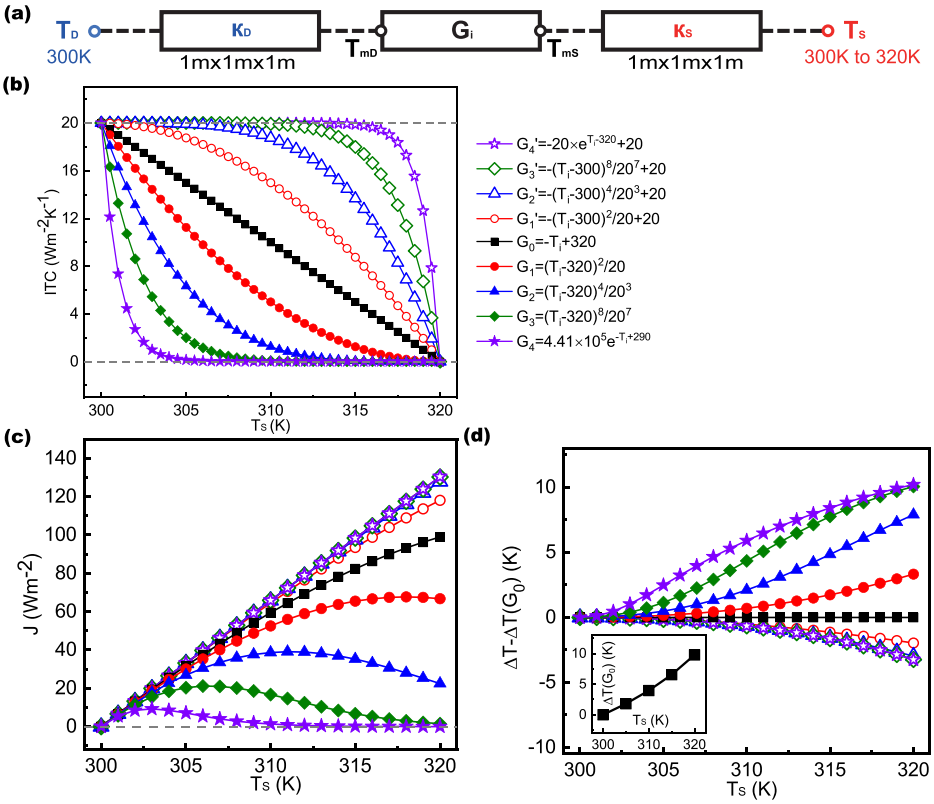

FIG. 1. The homogeneous junction with various ITCs is used to determine the conditions for the occurrence of NDTR effects. (a) Thermal circuit diagram of a two-terminal system with ITC. (b) The schematic diagram of the various ITCs introduced in homogeneous junction. (c) Thermal flux in homogeneous junction when different ITCs are introduced. For ITC from G_1 to G_4, the NDTR effect appears in the homogeneous junction. (d) Based on the G_0 case, the relative change of temperature difference between the interface under various ITCs. The temperature difference between the interface for the G_0 case is shown in the inset. When the NDTR effect appears in the homogeneous junction, the temperature difference between the interface increases significantly.

side of Fig. 1(b). Since the homojunction is taken as an example in this paper, the interfacial temperature T_i is defined as $T_i = (T_{mS} + T_{mD})/2$. The previous study indicated that the INDTR may occur in the system only when the temperature-dependent coefficient of ITC is greater than 1.[56] Through our numerical calculations, the concave temperature-dependent characteristic of ITC is proven to be another necessary condition to realize the INDTR. Here, we introduce the various ITCs in the homogeneous junction, such as power drop and exponential drop, all of which have the temperature-dependent coefficient higher than 1, as shown in Fig. 1(b). For the material used in the drain terminal and source terminal, they are assumed to have the same form as follows:

$$\kappa_D(T) = \kappa_S(T) = \frac{600}{T}. \tag{3}$$

In the calculation, we set $L_D = L_S = 1$ m. The cross section of the homojunction is a square with a side length of 1m. The temperature of the drain terminal T_D is set at 300 K. By using the finite element simulations (COMSOL-MULTIPHYSICS software), the thermal flux in the homojunction and the temperature difference at the interface are shown in Figs. 1(c) and 1(d), respectively. For the TDITC with a concave function form, the INDTR is easily observed, whereas it does not exist for the convex function form, indicating that the rapid drop characteristic of ITC near drain temperature is the main reason for achieving INDTR (see Sec. S2 in the supplementary material for the theoretical verification). Meanwhile, as shown in Fig. 1(d), in the form of convex function, the interfacial temperature difference is obviously small, and the ITC is always in a high conduction state. In addition, another thing to be noted is that the maximum value of thermal flux and its corresponding temperature are closely related to the decrease rate of ITC near the drain temperature. Overall, the ITC near the drain terminal decrease at a rate from the 4th to the 8th power can achieve the optimal INDTR.

An obvious INDTR could directly enable to design thermal transistors. In Fig. 2(a), a schematic diagram of the thermal transistor based on INDTR is given, similar to the electronic transistor, and the gate terminal is introduced to realize the control function of the thermal transistor. According to the continuity equation (conservation conditions of thermal flux) in non-equilibrium steady state, the thermal flux can be expressed in the following expression:

$$J_D = \frac{1}{L_D}\int_{T_D}^{T_{mD}} \kappa_D(T)\ dT = \frac{(T_{mS} - T_{mD})}{R_i(T_{mS}, T_{mD})} = J_G + J_S$$
$$= \frac{1}{L_G}\int_{T_{mS}}^{T_G} \kappa_G(T)\ dT + \frac{1}{L_S}\int_{T_{mS}}^{T_S} \kappa_S(T)\ dT, \tag{4}$$

where G represents the abbreviation of gate terminal, and all the other symbols are same as those in Eq. (2). In particular, the TDITC between gate materials and source materials is not considered in Eq. (4). Since the main function of gate terminal is to regulate the interfacial temperature, so the ITC can be kept constant and small by the vertically external pressure and thermal interfacial materials. For the material of three terminals, we assume they have the same form as follows:

$$\kappa_G(T) = \kappa_D(T) = \kappa_S(T) = \frac{600}{T}. \tag{5}$$

In calculation, we set $L_D = 0.02$ and $L_S = L_G = 1$ m. The cross section of the homojunction is also considered to be a square with a side

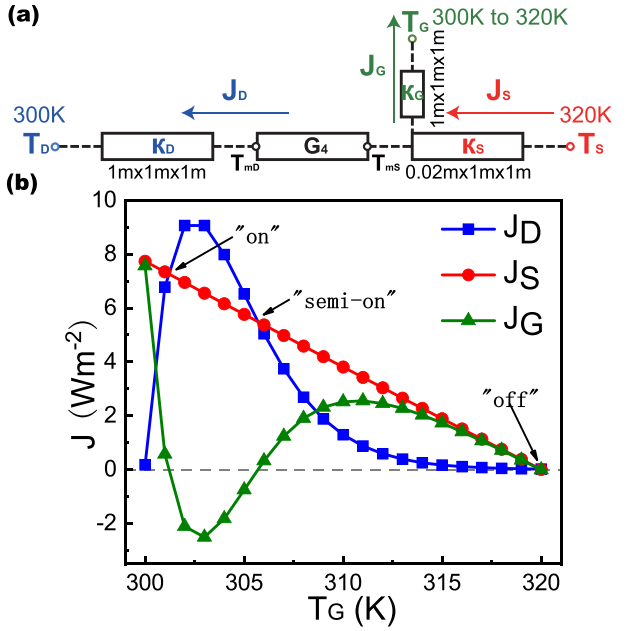

FIG. 2. Schematic diagram and characteristic curve of thermal transistor. (a) Thermal circuit diagram of a thermal transistor. (b) A typical characteristic curve of thermal transistor: Thermal flux in source terminal J_S, drain terminal J_D, and gate terminal J_G as a function of the temperature of the gate terminal T_G. In the calculation, the temperatures of source terminal T_S and drain terminal T_D are set at 320 and 300 K, respectively.

length of 1m. The temperatures of source terminal T_S and drain terminal T_D are set at 320 and 300 K, respectively. Here, the ITC with the form of G_4 is selected as an example to study transport property of the thermal transistor by using the finite element calculation, and the characteristic curve of the thermal transistor is shown in Fig. 2(b). With the introduction of ITC at the three-terminal system, the INDTR occurs at the interface, which makes the thermal flux in gate material J_G and drain material J_D responds non-monotonically when the temperature of gate terminal T_G increases monotonically. Therefore, the monotonic thermal flux in the source material J_S and the thermal flux in the drain material J_D will be equal at the three special temperatures of gate terminal T_G. That is to say, the thermal flux in the gate material J_G is 0 here, which will not play any role in the thermal transport, so that the thermal flux from the source terminal would completely flow into the drain terminal. Naturally, we can define the thermal flux from the source terminal to the drain terminal J_{SD} as

$$J_{SD} = J_S = J_D. \tag{6}$$

These three special temperatures of gate terminal correspond to the three working states of the thermal transistor: on state, semi-on state, and off state, respectively. Naturally, by changing the temperature of the gate terminal T_G, the thermal flux in drain material J_D can be tuned in a controlled way.

The basic function of a thermal transistor is the ability of thermal switching; by just adjusting the temperature of gate terminal T_G, it can achieve turn-on or turn-off from the source terminal to the drain

terminal J_{SD}, like the MOSFET in digital circuits. As shown in Fig. 2(b), the off state can be found directly at $T_{off} = 319.97$ K, when the system can be regarded as a thermal insulator, with a thermal flux $J_{SD}^{off} = 0.013$ W m^{-2}. Meanwhile, the on state and semi-on state of the thermal transistor work at $T_{on} = 301.22$ and $T_{semi-on} = 305.70$ K, respectively, and the working thermal flux is $J_{SD}^{on} = 7.26$ and $J_{SD}^{semi-on} = 5.45$ W m^{-2}, respectively. At this point, the thermal flux in the on state J_{SD}^{on} is almost 550 times larger than that in the off state (J_{SD}^{off}), showing a gate-controlled thermal switching function with high performance. Here and in the following, the physical dimensions of the model are set as shown in Fig. 2(a) without any special emphasis. The temperatures of source terminal T_S and drain terminal T_D are always set at 320 and 300 K, respectively.

As shown in Fig. 3(a), when the thermal resistance of the source material is reduced, the thermal flux J_S is increased, and the switching function of the thermal transistor can be further enhanced. In order to realize the optimal switching function, thermal flux in the source material J_S is regulated by changing the length of the source material L_S, thus directly changing the thermal flux J_{SD} on the on state, and the results are shown in Fig. 3(b). When the length of the source material L_S is short, the thermal flux that comes from source terminal J_S is almost leaked by the gate terminal, and the thermal flux in the drain material J_D is almost 0, leading to the failure of the thermal transistor. There are also some problems with the source material like being too long, and it would no longer participate in the thermal transport process of the thermal transistor; therefore, the thermal flux J_{SD} for the on state is almost 0. The optimal length source material L_S in this thermal transistor model is optimized to 36.5 m, at which point, the thermal switching ratio $\gamma = J_{SD}^{on}/J_{SD}^{off}$ is enhanced to 700. In addition, since the drain terminal is directly connected to the source terminal, according to Eq. (1), increasing the length of drain terminal L_D will weaken the thermal flux J_D, which is consistent with the effect of reducing the length of source terminal on the thermal transistor.

The thermal switching function denotes that the thermal transistor could work as an insulator or a conductor by controlling the temperature of the gate terminal T_G. However, in many thermal management applications, we need not only a thermal switch with an on or off states but also a continuously adjustable thermal amplifier or thermal modulator with a wide thermal flux operating range. A characteristic curve of a typical thermal amplification function is shown in Fig. 3(c). In the calculation, the temperatures of source terminal T_S and drain terminal T_D are set at 310 and 300 K, respectively. When the temperature of gate terminal T_G is from 302.5 to 308.5 K, the thermal flux in the source material J_S decreases linearly and flows almost completely into the drain terminal. In the control region in Fig. 3(c), the average thermal flux in gate material $\overline{J_G}$ is about 0.11 W m^{-2}, much less than the thermal flux J_{SD}. At this point, the gate terminal is only used to control the thermal flux J_{SD}, which does not tune the thermal flux from the source terminal.

From Figs. 3(a) and 3(c), we can find that the switching ratio γ mainly depends on the NDTR effect, and it also determines the maximum range of the thermal modulation function. When the material and ITC of the multi-terminal system are determined, the maximum switching ratio and the maximum range of the thermal modulation function are also determined, so an optimal thermal modulation function naturally requires the minimization of thermal flux in gate material J_G. In Fig. 3(d), we find the optimal thermal modulation effect of

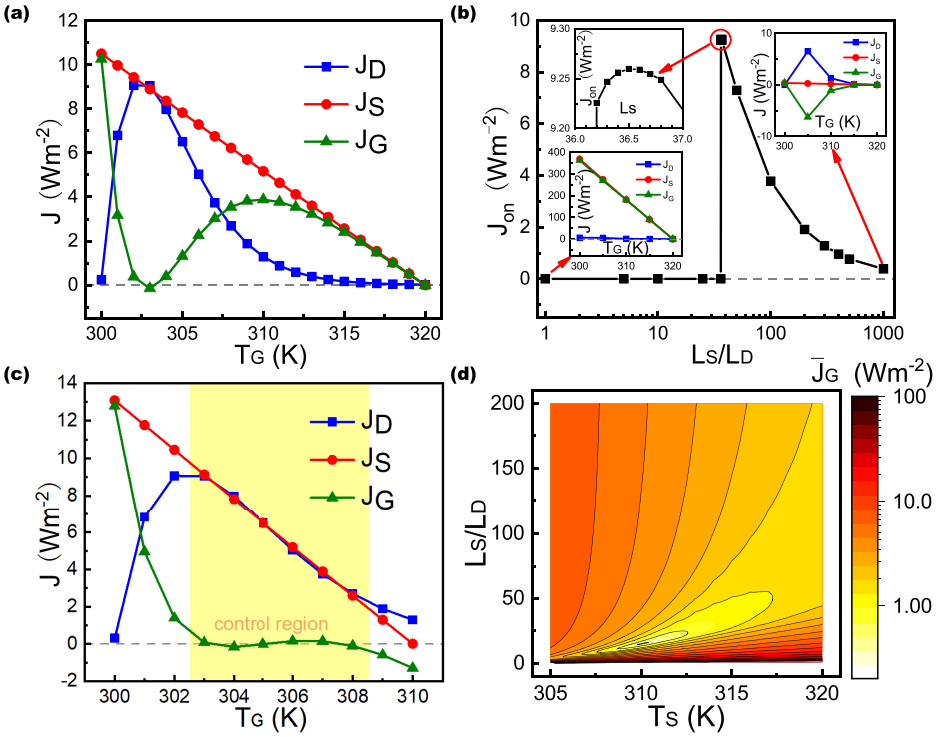

FIG. 3. (a) A typical characteristic curve of the thermal switching function in an optimized thermal transistor. In the calculation, the temperatures of source terminal T_S and drain terminal T_D are set at 320 and 300 K, respectively. (b) The thermal flux on the state J_{on} as a function of the length of the source material L_S. The inset shows the characteristic curve of the thermal transistor in the case of excessively long and excessively long source material. (c) A typical characteristic curve of the thermal amplification/modulation function in an optimized thermal transistor. In the calculation, the temperatures of source terminal T_S and drain terminal T_D are set at 310 and 300 K, respectively. (d) The average thermal flux in gate material under the control region $\overline{J_G}$ is a function of the length ratio L_S/L_D and the temperature of the source terminal T_S.

this thermal transistor by changing the length of the source material L_S and the temperature of the source terminal T_S, where the optimal parameter is $T_S = 310.1$ K and $L_S = 15.3$ m. In particular, if the length of the source material L_S is too long, the thermal flux of the source terminal J_S is too small, resulting in that the gate terminal will participate in the transport process. At the same time, if the temperature of the source terminal T_S is too low, the temperature difference between the interface would be very small, resulting in the disappearance of NDTR.

According to the INDTR discussed earlier, we reproduce the thermal switching function and thermal amplification function in a macroscopic thermal transistor based on a bulk silicon homojunction. Silicon was chosen because of its NTE characteristic at low temperature (<120 K),[58] and the accompanying INDTR will occur in silicon homojunction, which provides a prospect for the development of thermal transistors.[56] The schematic diagram of Si homogenous junction is similar to Fig. 2(a), which consists of three segments, all of which are bulk Si, and the relevant material property settings are the same as those in Ref. 56. In particular, the ITC as described in the previous work[56,57] is also chosen in the following form:

$$G_i = C_1 \tanh(PS/C_2) + C_3, \tag{7}$$

where P and S represent the total pressure and the cross-sectional area at the interface, respectively. C_1, C_2, and C_3 in Eq. (7) are variables used to adjust the value of the ITC under high- or low-pressure limit. In this work, the values of C_1, C_2, and C_3 are set as 4000 W m^{-2} K^{-1}, 5 kg·m s^{-2}, and 3700 W m^{-2} K^{-1}, respectively. The geometric parameters of the source terminal and drain terminal are set as $20 \times 2 \times 0.5\,\text{mm}^3$ and $61.5 \times 2 \times 0.5\,\text{mm}^3$, respectively. Here, the geometric parameters of gate terminal are $0.5 \times 2 \times 0.5\,\text{mm}^3$, and the gate terminal is gravitationally attached to the source terminal vertically at 0.5 mm away from the interface. Because of the vertical stacking of gate terminal and source terminal, we do not consider TDITC here either. According to the temperature range of the NTE characteristics of Si, the temperatures of source terminal T_S and drain terminal T_D are set to be 120 and 100 K, respectively.

The characteristic curve of the Si thermal transistor is shown in Fig. 4. The thermal flux $J_{SD}^{on} = 176.58$ kW m^{-2} is 33 times of the thermal flux $J_{SD}^{off} = 5.31$ kW m^{-2}, which can achieve a good thermal switching function. In the whole temperature range between the temperature of turn-on state ($T_{on} = 105.5$ K) and turn-off state ($T_{off} = 120$ K), the Si thermal transistor embodies an excellent thermal modulation function. The thermal flux J_{SD} is basically linearly and monotonously regulated by the temperature of gate terminal T_G, and the working leakage ratio in gate terminal $\delta = \overline{J_G}/J_{SD}^{on}$ is only 2.04%. These results indicate that the Si transistors have an excellent thermal switching function and thermal amplification/modulation function, which proves that thermal transistors designed based on INDTR can achieve precise and high-performance thermal management and thermal control.

In summary, we design and optimize a high-performance thermal transistor based on the INDTR. First, the conditions for the INDTR in the multi-terminal system are determined as follows: the temperature-dependent coefficient of ITC should be greater than 1, and the ITC should be concave dependent on the temperature. Then, we design a thermal transistor and calculate the thermal transport characteristic curve in a three-terminal system with INDTR.

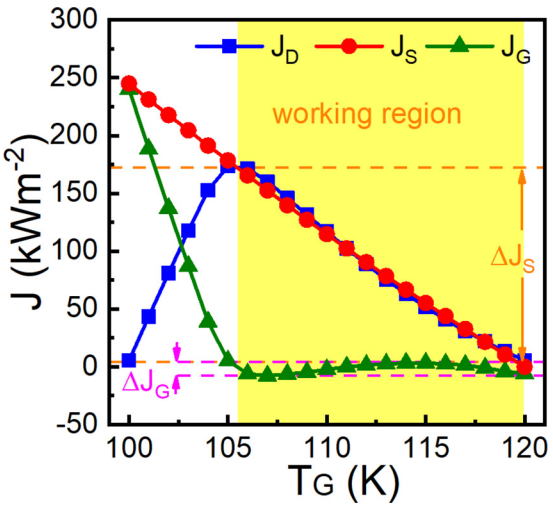

FIG. 4. Characteristic curve of thermal transistor based on bulk Si homogeneous junction. The on–off ratio corresponding to the thermal switching function is indicated by the orange arrow, and the working region of the thermal amplification function is shown in the yellow region.

Meanwhile, an easily applicable and universal method for optimizing the switching function and amplifying function of the thermal transistor is proposed and discussed. As a practical analogue, we have discussed a high-performance thermal transistor with an on–off ratio of 33 and a leakage ratio in gate terminal of less than 2.04% in the Si homojunction at low temperature. Our work provides an efficient and convenient way to design and optimize high-performance thermal devices, thus paves the way to regulate and manage the thermal transport process precisely, flexibly, and functionally.

See the supplementary material for more introductions, proofs, and discussions of the INDTR and TDITC.

This work was supported by the National Natural Science Foundation of China (Grant Nos. 11975125, 11890703, and 12204244), the Natural Science Foundation of Jiangsu Province (Grant No. BK20210556), and the Department of Science and Technology of Jiangsu Province (No. BK20220032). Z.Y.S. acknowledges support from the Jiangsu Specially-Appointed Professor Program. Y.Y. acknowledges support from the Postgraduate Research & Practice Innovation Program of Jiangsu Province (Grant No. KYCX22 1539).

AUTHOR DECLARATIONS

Conflict of Interest

The authors have no conflicts to disclose.

Author Contributions

Yu Yang: Conceptualization (equal); Formal analysis (equal); Funding acquisition (equal); Investigation (equal); Methodology (equal); Validation (equal); Visualization (equal); Writing – original draft (equal);

Writing – review & editing (equal). **Yunshan Zhao:** Conceptualization (equal); Formal analysis (equal); Funding acquisition (equal); Investigation (equal); Methodology (equal); Resources (equal); Supervision (equal); Validation (equal); Visualization (equal); Writing – original draft (equal); Writing – review & editing (equal). **Lifa Zhang:** Conceptualization (equal); Formal analysis (equal); Funding acquisition (equal); Investigation (equal); Methodology (equal); Resources (equal); Supervision (equal); Validation (equal); Visualization (equal); Writing – original draft (equal); Writing – review & editing (equal).

DATA AVAILABILITY

The data that support the findings of this study are available from the corresponding authors upon reasonable request.

REFERENCES

[1]M. Waldrop, Nature **530**, 144–147 (2016).
[2]Q. Wang, B. Jiang, B. Li, and Y. Yan, Renewable Sustainable Energy Rev. **64**, 106–128 (2016).
[3]N. Li, J. Ren, L. Wang, G. Zhang, P. Hänggi, and B. Li, Rev. Mod. Phys. **84**, 1045–1066 (2012).
[4]S. Sklan and B. Li, Nat. Sci. Rev. **5**, 138–141 (2018).
[5]Y. Li, W. Li, T. Han, X. Zheng, J. Li, B. Li, S. Fan, and C.-W. Qiu, Nat. Rev. Mater. **6**, 488–507 (2021).
[6]C. Z. Fan, Y. Gao, and J. P. Huang, Appl. Phys. Lett. **92**, 251907 (2008).
[7]S. Narayana and Y. Sato, Phys. Rev. Lett. **108**, 214303 (2012).
[8]R. Schittny, M. Kadic, S. Guenneau, and M. Wegener, Phys. Rev. Lett. **110**, 195901 (2013).
[9]Z. Zhang, Y. Guo, M. Bescond, J. Chen, M. Nomura, and S. Volz, APL Mater. **9**, 081102 (2021).
[10]T. Vasileiadis, J. Varghese, V. Babacic, J. Gomis-Bresco, D. Navarro Urrios, and B. Graczykowski, J. Appl. Phys. **129**, 160901 (2021).
[11]M. Terraneo, M. Peyrard, and G. Casati, Phys. Rev. Lett. **88**, 094302 (2002).
[12]B. Li, L. Wang, and G. Casati, Phys. Rev. Lett. **93**, 184301 (2004).
[13]B. Li, J. Lan, and L. Wang, Phys. Rev. Lett. **95**, 104302 (2005).
[14]Y. Yang, H. Chen, H. Wang, N. Li, and L. Zhang, Phys. Rev. E **98**, 042131 (2018).
[15]C. W. Chang, D. Okawa, A. Majumdar, and A. Zettl, Science **314**, 1121–1124 (2006).
[16]H. Wang, S. Hu, K. Takahashi, X. Zhang, H. Takamatsu, and J. Chen, Nat. Commun. **8**, 15843 (2017).
[17]B. Li, L. Wang, and G. Casati, Appl. Phys. Lett. **88**, 143501 (2006).
[18]W. Chung Lo, L. Wang, and B. Li, J. Phys. Soc. Jpn. **77**, 054402 (2008).
[19]Q. Ruan and L. Wang, Phys. Rev. Res. **2**, 023087 (2020).
[20]P. Ben-Abdallah and S.-A. Biehs, Phys. Rev. Lett. **112**, 044301 (2014).
[21]I. Latella, O. Marconot, J. Sylvestre, L. G. Fréchette, and P. Ben-Abdallah, Phys. Rev. Appl. **11**, 024004 (2019).
[22]E. Moncada-Villa and J. C. Cuevas, Phys. Rev. Appl. **15**, 024036 (2021).
[23]J. Ren and J.-X. Zhu, Phys. Rev. B **87**, 241412 (2013).
[24]K. Joulain, J. Drevillon, Y. Ezzahri, and J. Ordonez-Miranda, Phys. Rev. Lett. **116**, 200601 (2016).
[25]C. Wang, X.-M. Chen, K.-W. Sun, and J. Ren, Phys. Rev. A **97**, 052112 (2018).
[26]B.-Q. Guo, T. Liu, and C.-S. Yu, Phys. Rev. E **98**, 022118 (2018).
[27]J. Yang, C. Elouard, J. Splettstoesser, B. Sothmann, R. Sánchez, and A. N. Jordan, Phys. Rev. B **100**, 045418 (2019).
[28]B.-Q. Guo, T. Liu, and C.-S. Yu, Phys. Rev. E **99**, 032112 (2019).
[29]H. Liu, C. Wang, L.-Q. Wang, and J. Ren, Phys. Rev. E **99**, 032114 (2019).
[30]M. Majland, K. S. Christensen, and N. T. Zinner, Phys. Rev. B **101**, 184510 (2020).
[31]J. Lu, R. Wang, C. Wang, and J.-H. Jiang, Phys. Rev. B **102**, 125405 (2020).
[32]R. Ghosh, A. Ghoshal, and U. Sen, Phys. Rev. A **103**, 052613 (2021).
[33]A. Mandarino, K. Joulain, M. D. Gómez, and B. Bellomo, Phys. Rev. Appl. **16**, 034026 (2021).
[34]R. T. Wijesekara, S. D. Gunapala, and M. Premaratne, Phys. Rev. B **104**, 045405 (2021).
[35]A. Fornieri, G. Timossi, R. Bosisio, P. Solinas, and F. Giazotto, Phys. Rev. B **93**, 134508 (2016).
[36]N. Yang, N. Li, L. Wang, and B. Li, Phys. Rev. B **76**, 020301 (2007).
[37]Q. Ruan and L. Wang, Phys. Rev. E **107**, 044120 (2023).
[38]Z.-G. Shao, L. Yang, H.-K. Chan, and B. Hu, Phys. Rev. E **79**, 061119 (2009).
[39]W.-R. Zhong, P. Yang, B.-Q. Ai, Z.-G. Shao, and B. Hu, Phys. Rev. E **79**, 050103 (2009).
[40]D. He, S. Buyukdagli, and B. Hu, Phys. Rev. B **80**, 104302 (2009).
[41]D. He, B.-Q. Ai, H.-K. Chan, and B. Hu, Phys. Rev. E **81**, 041131 (2010).
[42]B.-Q. Ai and B. Hu, Phys. Rev. E **83**, 011131 (2011).
[43]B,-Q. Ai, W.-R. Zhong, and B. Hu, Phys. Rev. E **83**, 052102 (2011).
[44]W.-R. Zhong, M.-P. Zhang, B.-Q. Ai, and B. Hu, Phys. Rev. E **84**, 031130 (2011).
[45]H.-K. Chan, D. He, and B. Hu, Phys. Rev. E **89**, 052126 (2014).
[46]Y. Ming, H.-M. Li, and Z.-J. Ding, Phys. Rev. E **93**, 032127 (2016).
[47]R. Luo, Phys. Rev. E **99**, 032138 (2019).
[48]J. Hu, Y. Wang, A. Vallabhaneni, X. Ruan, and Y. P. Chen, Appl. Phys. Lett. **99**, 113101 (2011).
[49]X.-K. Chen, Z.-X. Xie, W.-X. Zhou, L.-M. Tang, and K.-Q. Chen, Carbon **100**, 492–500 (2016).
[50]X.-K. Chen, J. Liu, Z.-H. Peng, D. Du, and K.-Q. Chen, Appl. Phys. Lett. **110**, 091907 (2017).
[51]L. Castelli, Q. Zhu, T. J. Shimokusu, and G. Wehmeyer, Nat. Commun. **14**, 393 (2023).
[52]X. Shen, Y. Li, C. Jiang, and J. Huang, Phys. Rev. Lett. **117**, 055501 (2016).
[53]G. L. POLLACK, Rev. Mod. Phys. **41**, 48–81 (1969).
[54]E. T. Swartz and R. O. Pohl, Rev. Mod. Phys. **61**, 605–668 (1989).
[55]J. Chen, X. Xu, J. Zhou, and B. Li, Rev. Mod. Phys. **94**, 025002 (2022).
[56]Y. Yang, D. Ma, Y. Zhao, and L. Zhang, J. Appl. Phys. **127**, 195301 (2020).
[57]Y. Yang, X. Li, and L. Zhang, Chin. Phys. Lett. **38**, 016601 (2021).
[58]Y. H. Lee, R. Biswas, C. M. Soukoulis, C. Z. Wang, C. T. Chan, and K. M. Ho, Phys. Rev. B **43**, 6573–6580 (1991).